van der Waals epitaxy of monolayer hexagonal boron nitride on copper foil: growth, crystallography and electronic band structure

To cite this article: Grace E Wood *et al* 2015 *2D Mater.* **2** 025003

2D Materials

OPEN ACCESS

RECEIVED
20 January 2015

REVISED
6 March 2015

ACCEPTED FOR PUBLICATION
23 March 2015

PUBLISHED
6 May 2015

PAPER

van der Waals epitaxy of monolayer hexagonal boron nitride on copper foil: growth, crystallography and electronic band structure

Grace E Wood[1], Alexander J Marsden[1], James J Mudd[1], Marc Walker[1], Maria Asensio[2], Jose Avila[2], Kai Chen[2], Gavin R Bell[1] and Neil R Wilson[1]

[1] Department of Physics, University of Warwick, Coventry CV4 7AL, UK
[2] Synchrotron Soleil, L'Orme des Merisiers, Saint-Aubin, France

E-mail: Neil.Wilson@warwick.ac.uk

Keywords: monolayer hexagonal boron nitride, chemical vapour deposition, epitaxy, structural feedback, angle-resolved photoemission spectroscopy

Abstract

We investigate the growth of hexagonal boron nitride (*h*-BN) on copper foil by low pressure chemical vapour deposition (LP-CVD). At low pressure, *h*-BN growth proceeds through the nucleation and growth of triangular islands. Comparison between the orientation of the islands and the local crystallographic orientation of the polycrystalline copper foil reveals an epitaxial relation between the copper and *h*-BN, even on Cu(100) and Cu(110) regions whose symmetry is not matched to the *h*-BN. However, the growth rate is faster and the islands more uniformly oriented on Cu(111) grains. Angle resolved photoemission spectroscopy measurements reveal a well-defined band structure for the *h*-BN, consistent with a band gap of 6 eV, that is decoupled from the copper surface beneath. These results indicate that, despite a weak interaction between *h*-BN and copper, van der Waals epitaxy defines the long range ordering of *h*-BN even on polycrystalline copper foils and suggest that large area, single crystal, monolayer *h*-BN could be readily and cheaply produced.

1. Introduction

Interest in monolayer hexagonal boron nitride (*h*-BN) has been stimulated by its complementarity to graphene, with demonstrations of its use as a dielectric substrate to improve the mobility of graphene or as a tunnel barrier to add novel functionality to graphene devices [1]. It is iso-structural to graphene, with a lattice parameter only 1.8% larger, but is a wide band gap semiconductor rather than a semi-metal. As with graphene, the proof of principle experiments have utilized mechanically exfoliated *h*-BN flakes, but large scale application will require scalable synthesis of large area, high quality material.

Chemical vapour deposition (CVD) is proving to be a promising technique to fulfil this need. CVD of monolayer *h*-BN on single crystal substrates in ultra high vacuum (UHV) was reported in the 1990s [2], but due to the high cost of the substrate and UHV growth chamber it is not a practical source of material for applications. Following shortly after the CVD growth of graphene on copper foil [3], recent reports of *h*-BN growth on low cost substrates have shown the potential for CVD to be a low cost route to high quality monolayer or few layer *h*-BN [4–11]. CVD growth of *h*-BN proceeds through nucleation and growth of islands that merge to form a continuous film. As a result, similarly to graphene growth [12], CVD grown *h*-BN can form large area but polycrystalline films [10]. The grain boundaries within these films have distinct properties from the pristine layers which, though interesting in their own right [13], are undesirable for applications such as the use of *h*-BN as a dielectric substrate.

In layered materials such as graphene/graphite and transition metal dichalcogenides, the inter-layer attraction arises through dispersion forces (van der Waals bonding) rather than strong chemical bonds. Unlike conventional materials, they do not have out-of-plane dangling bonds at their surface: in conventional epitaxy, the dangling bonds on the substrate material result in the formation of strong chemical bonds that require a close lattice-match between substrate and growth material. By contrast, layered materials tend to interact with a surface of even a non-layered material via van der Waals bonding. As a

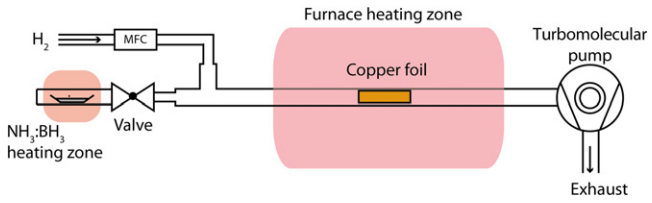

Figure 1. Schematic of the LP-CVD growth setup.

result, epitaxial growth can occur for these two-dimensional systems despite lattice mismatch and even without matching symmetry. This van der Waals epitaxy [14] can result in high quality, defect free material where the crystallographic orientation of the grown layer is still defined by that of the substrate. For graphene growth, it has been shown that under low-pressure conditions the orientation of the graphene grains can be determined by the substrate crystallography even on copper foil [15–17]. Under UHV conditions on single crystal substrates, *h*-BN has been shown to grow epitaxially on Cu(111), with the *h*-BN lattice orientationally aligned to the hexagonal Cu (111) surface lattice despite the significant (1.8%) lattice mismatch [18, 19]. However, to the best of our knowledge, there have been no systematic studies on whether this epitaxial alignment persists in the more technologically relevant CVD growth on low cost copper substrates where the surface is often not Cu(111). Understanding and controlling the epitaxial growth of *h*-BN should allow large area, monolayer, single crystal *h*-BN to be grown without the presence of grain boundaries yielding higher quality material.

In this paper we demonstrate the low pressure CVD (LP-CVD) growth of *h*-BN from ammonia borane feedstock. Scanning electron microscopy (SEM) shows that independently nucleated islands large distances from one another are frequently aligned in the same orientation. Determination of the copper crystallography by electron backscatter diffraction (EBSD), correlated to quantification of the island orientations, suggests that this alignment is due to interaction with the copper surface. It is noticeable that the epitaxial alignment is more prominent on Cu (111) regions and that the typical island sizes there are larger. AFM shows that the copper surface restructures and facets under the monolayer *h*-BN, but angle resolved photoemission spectroscopy (ARPES) shows the band structure of the *h*-BN is electronically decoupled from the copper indicating only a weak interaction.

2. Methods

LP-CVD of h-BN. Copper foils (99.5% purity, 0.025 mm thick, Alfa Aesar 46365) were cleaned by electropolishing (10 s at 5 V, ~1.5 A) in an electrolyte containing orthophosphoric acid and urea, followed by rinsing in acetone and isopropanol. The foil was loaded to the centre of a 1 inch diameter quartz work tube inside a split tube furnace, evacuated down to a base pressure of $<10^{-7}$ mbar using a turbo pump backed by a dry diaphragm pump, then heated to 1000 °C under a flow of 10 standard cubic centimeters (sccm) of hydrogen (99.9995%). The foil was annealed for 10 min at 1000 °C prior to growth. 15 mg of ammonia borane (97% purity, Sigma Aldrich 682098) was placed in a quartz boat in a small chamber, separated from the furnace by a valve, and independently heated using heating tape. Growth was initiated by opening the valve to the ammonia borane, no hydrogen was flowed during growth. After growth, hydrogen flow was resumed and the furnace cooled to <200 °C before removing the foil.

SEM, EBSD and AFM. SEM images were taken on a Zeiss Supra 55-VP FEGSEM operating at 10 kV with the Inlens detector. The same instrument was used for EBSD measurements, using an EDAX EBSD system. AFM images were taken with an Asylum Research MFP3D-SA operated in AC (tapping) mode.

Photoemission. ARPES and XPS measurements were taken at the Antares beamline at Synchrotron Soleil using a Scienta R4000 electron analyser with 2D detection [20]. A photon energy of 700 eV was used for XPS measurements, and of 100 eV for ARPES measurements. The binding energy scale was calibrated using the copper Fermi edge.

3. Results and discussions

A schematic of the experimental set-up used here for LP-CVD of *h*-BN is shown in figure 1, similar to that used by Ismach *et al* [4]. Ammonia borane was used as a stoichiometric source of boron and nitrogen; it was contained in a small chamber, separated from the growth furnace by a valve, with independent temperature control.

As shown in the SEM images in figure 2, characteristically triangular *h*-BN islands nucleate independently and grow, with the average island size increasing with growth time. Under the conditions used here, the islands start to coalesce after around 20 min and a continuous *h*-BN sheet is formed after 60 min. At this stage, small white triangles and white lines can be observed in the SEM images, indicative of multi-layer regions and wrinkles respectively. The

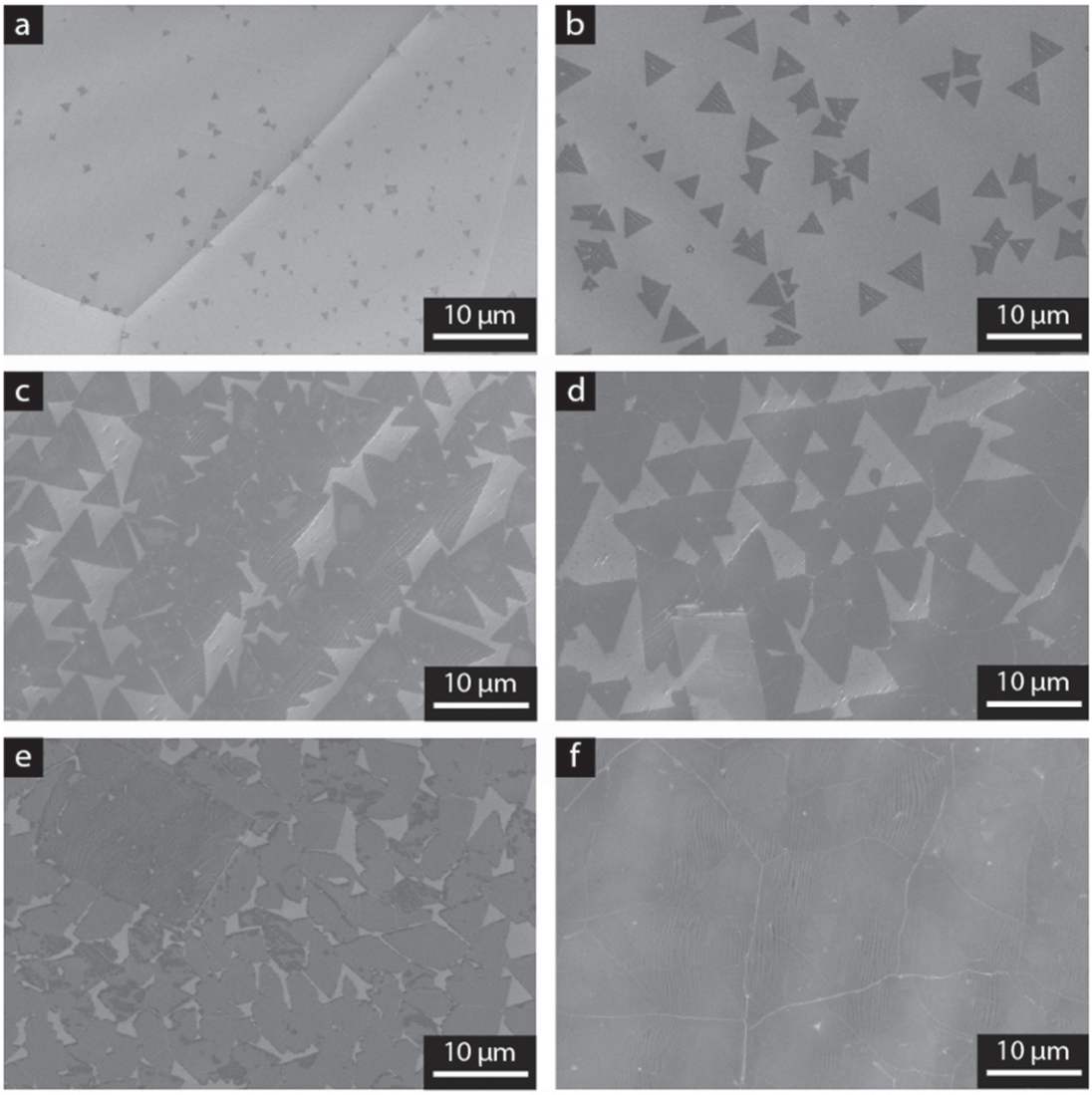

Figure 2. SEM of LP-CVD growth with growth times of (a) 10 min, (b) 15 min, (c) 20 min, (d) 30 min, (e) 40 min and (f) 60 min.

typical island size here when coalescence starts is $\sim 10\,\mu$m or $\sim 50\,\mu$m^2. The growth rate appears to decrease over time, consistent with a copper surface catalysed reaction.

The triangular islands are strongly indicative of *h*-BN growth, consistent with zigzag nitrogen terminated edges as the most energetically favourable configuration under these conditions [21]. However, it should be noted that under other growth conditions, e.g. higher partial pressures of the active B-N species, the island shape can deviate from triangular, with reports for example of hexagonal islands in atmospheric pressure CVD of *h*-BN on copper foils [6, 7]. Here the presence of *h*-BN is confirmed by XPS measurements (see supporting information). Even though we have not performed a systematic optimization of the growth conditions, the island size here is similar to or larger than that reported by Tay *et al* [6]. In agreement with their results, we found that electropolishing the copper foil prior to use was essential for reproducible growth of such larger islands.

Previous reports of *h*-BN growth from ammonia borane precursor have found significant deposition of BN particulates, which could be mostly removed by filters between the ammonia borane and growth furnace [9]. However, no particulates are apparent in these SEM images and this is further verified by AFM (see later). The lower ammonia borane temperature used here, and the separation of the ammonia borane to a small side chamber, result in a clean growth.

A striking feature of the triangular islands in figure 2 is that despite nucleating independently, i.e. the nucleation of one island is not determined by another, they often have the same orientation. Prior reports have also noted that the triangles appear to be aligned, but have not investigated this effect further [9, 17].

In the SEM image shown in figure 3(a), triangular *h*-BN islands can be seen on three copper grains. The darker, more circular regions are graphene: unfortunately, we occasionally found that *h*-BN growth was contaminated with graphene, despite no hydrocarbon

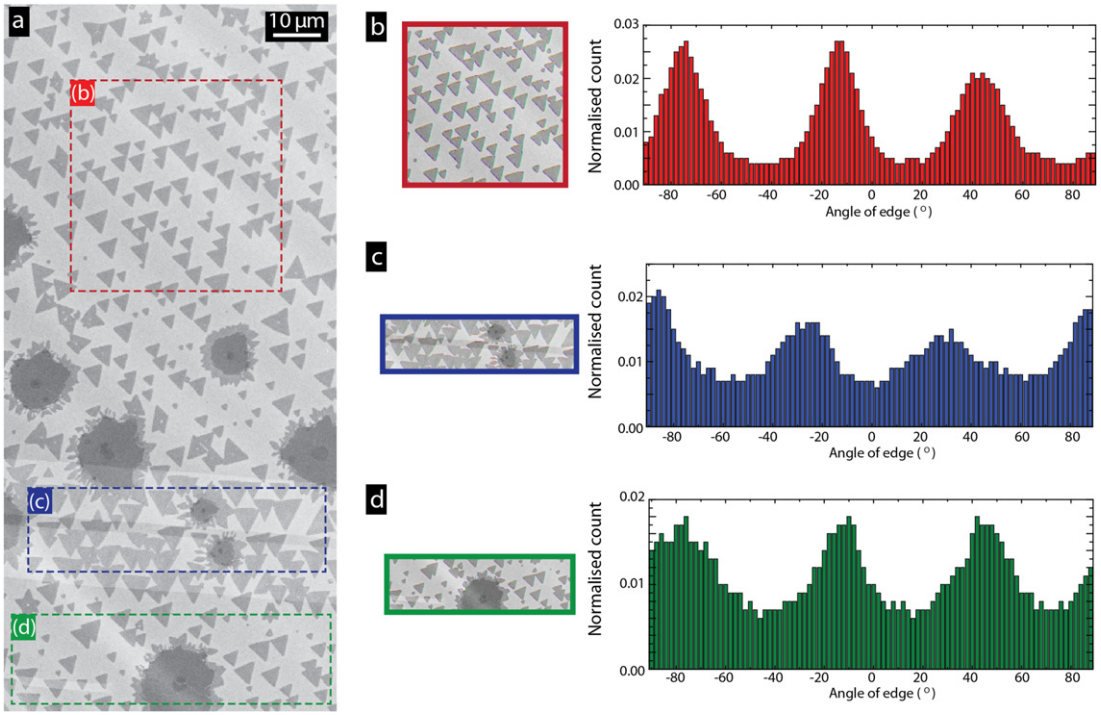

Figure 3. (a) SEM image of copper foil with triangular *h*-BN islands. Panels (b)–(d) show directionality analysis of the sections of image as indicated, revealing the preferred orientation of the triangular islands in each.

being deliberately introduced to the system. Strudwick *et al* have shown that copper foils can contain small amounts of carbon that during annealing in hydrogen can precipitate as graphene, with the amounts varying from foil to foil [22]. This could explain the growth of graphene here without an external carbon source and is consistent with the graphene forming before *h*-BN growth as *h*-BN can be seen to grow from the graphene islands but not the reverse. We note that most *h*-BN islands nucleate and grow separately from the graphene islands, and hence the presence of small fractions of graphene in some of these samples does not compromise the conclusions drawn below on the orientations of the *h*-BN islands. We have found that graphene and *h*-BN can be easily distinguished in the SEM by their different contrast, particularly in multi-layer regions. In conventional secondary electron detection images, wrinkles and multi-layer islands are dark for graphene but light for *h*-BN [23].

The dashed boxes on figure 3(a) mark sections of the image from the three different copper grains. In each, the triangular *h*-BN islands appear to be orientated in a consistent direction. Closer inspection suggests that the orientation of *h*-BN islands in the middle copper grain, marked by the dashed blue rectangle, is in a slightly different direction to the other two.

Image analysis was used to robustly and independently quantify the orientations of the triangular *h*-BN islands in the SEM images, using the directionality plugin for the ImageJ analysis software [24]. This measures the orientations of edges within an image, producing histograms of the total amount (i.e. length) of edges at a given angle. For a single equilateral triangle this would result in three equal height peaks in the histogram separated by 60°. The histograms in figures 3(b)–(d) show the edge orientations from sections of the three different copper grains shown in the corresponding SEM images. In each histogram three peaks can be observed, separated by 60° as expected, indicating the preferred orientation of the triangular islands in each image. However, from the histograms it is clear that there is a roughly 10° difference in the orientation of the islands in (c) compared to those in (b) and (d). The observation that the preferred orientation changes from one grain to the next and back again is not consistent with the orientation being determined by the gas flow direction, as suggested by Han *et al* [9], but rather indicates that it is due to interaction with the substrate.

The importance of the interaction between *h*-BN and copper surface can also be seen in AFM topography images, as shown in figure 4. The copper surface has restructured under the *h*-BN monolayer, forming sharply angled corrugations. This interfacial restructuring is similar to that observed for graphene on copper [15]. As in the case of graphene on copper [15], for partial coverage of *h*-BN this structural feedback facetting effect is *only* seen on areas of the sample covered by *h*-BN. The faceting extends across large areas, as shown in figures 4(c) and (f). It appears that where the average surface plane is close to a crystallographic low-index face such as (100), the interaction with *h*-BN stabilizes facetting to that (lower energy) crystallographic face such that the surface orientation

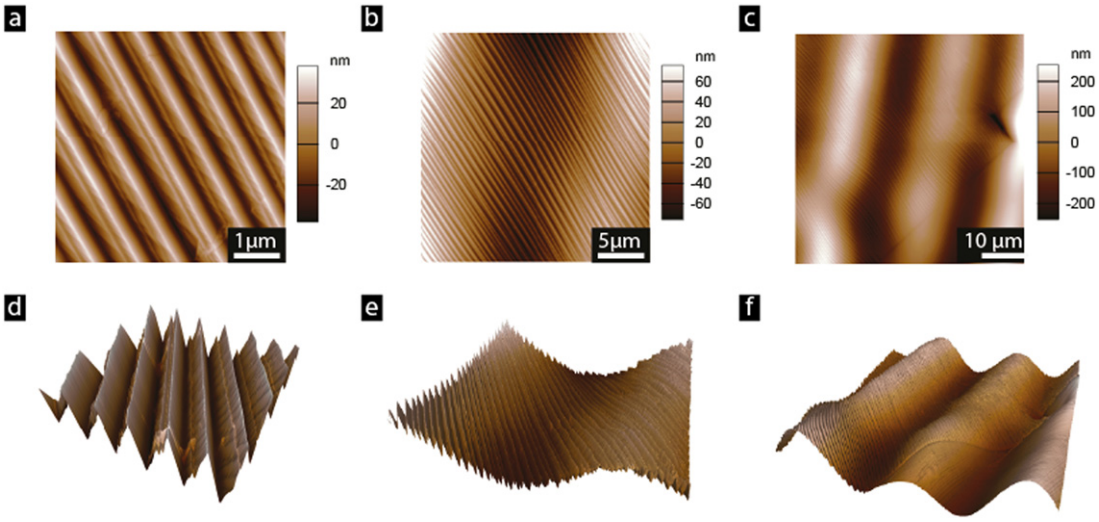

Figure 4. AFM topography images of *h*-BN on copper foil, the *h*-BN here fully covers the graphene surface. Panels (d)–(f) are the corresponding three-dimensional views of the surface topographies shown in (a)–(c).

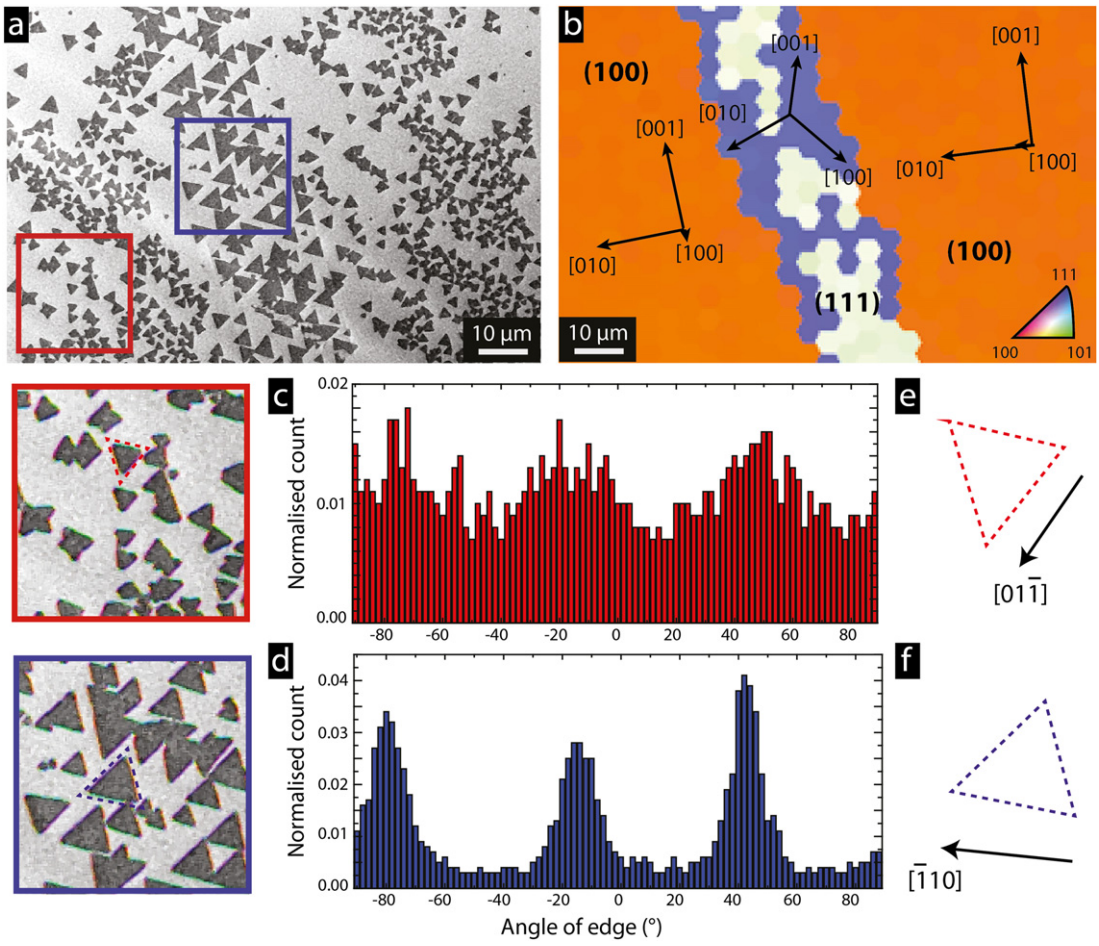

Figure 5. EBSD and SEM of *h*-BN on copper.(a) SEM image and (b) EBSD of the same area. Marked on are the orientations of the grains. Panels (c) and (d) are histograms of the edge orientations from selected areas of the SEM images, as indicated. The triangles shown in (e) and (f) are indicative of the orientations of the islands, as shown by the dashed triangles in (c) and (d) respectively; the arrows show crystallographic directions extracted from the EBSD data in (b) for the respective copper grains.

is predominantly (100). A detailed analysis of the energetic balance for such structural feedback is beyond the scope of the present paper.

EBSD was used to investigate the crystallography of the copper foil and compared to SEM images to determine the correlation between substrate

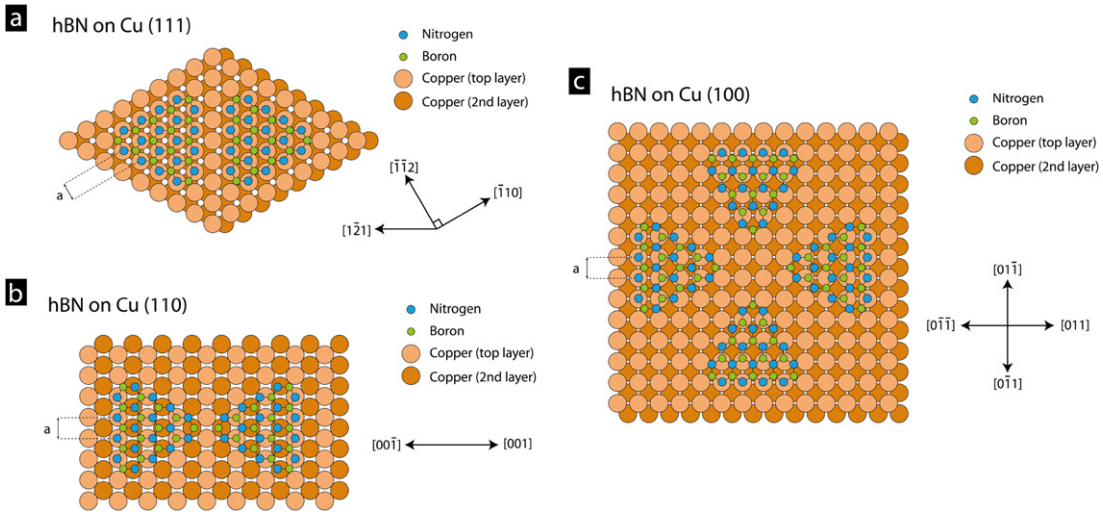

Figure 6. Atomic structure of monolayer *h*-BN on different orientations of copper surface, showing the top two atomic layers of each copper surface orientation. Panel (a) is for *h*-BN on Cu(111), (b) *h*-BN on Cu(110), and (c) *h*-BN on Cu(100).

crystallography and *h*-BN island orientation. EBSD shows that after growth the copper foil is polycrystalline but with macroscopic copper grains with lateral dimensions of typically millimeters or larger. The surface orientation is mostly aligned near Cu(100), but with Cu(111) microstripe inclusions (see supporting information), as previously reported for these copper foils after graphene growth [15] and [25]. An example is shown in figure 5 where EBSD and SEM of the same region reveals correlation between the orientation of the triangular islands and the copper surface orientation. EBSD reveals a Cu(111) microstripe between two vicinal Cu(100) regions. The *h*-BN islands are clearly larger on the Cu(111) region and are aligned relative to one another. The directionality analysis of this region, figure 5(d), quantitatively shows this. Comparison between the typical triangle orientation and the surface crystallography shows that the islands are aligned with one edge parallel to the Cu $[\bar{1}10]$ direction (extracted from the EBSD data), as shown in figure 5(f). Analysis of the island orientations on the Cu(100) region is more complicated in this image, but careful inspection shows that islands frequently have an edge parallel to the Cu $[01\bar{1}]$ direction, as shown in figures 5(c) and (e).

The correlation between the crystallography of the copper substrate and *h*-BN island orientation suggests that the copper surface is playing an important role. The growth of *h*-BN on copper is thought to involve surface mediated processes, with evidence that there is also some B diffusion through the bulk of the copper [11]. The islands nucleate and grow during the flow of ammonia-borane feedstock, whilst the copper foil is at 1000 °C. At this temperature, it is known that the copper surface is mobile [26], but despite this previous studies of graphene growth on copper under similar conditions have found that the crystallography of the copper surface still plays an important role in defining the orientation of the graphene [15, 16].

In order to understand the relation between the *h*-BN island orientations and the surface crystallography, it is necessary to consider the copper surface crystallography. Figure 6 shows the atomic arrangements of the Cu(111), Cu(110) and Cu(100) surfaces, with *h*-BN islands overlaid. The bulk structure of copper is face centred cubic (fcc), with a room temperature lattice parameter of $a_{Cu} = 0.361$ nm.

The Cu(111) surface has hexagonal symmetry, with surface lattice parameter of $a = a_{Cu}/\sqrt{2} = 0.255$ nm, as shown in figure 6(a). The in plane room temperature lattice parameter of *h*-BN is 0.250 nm, 1.8% smaller than the copper surface lattice. Density functional calculations have predicted that the N atoms reside on top of the surface metal atoms whereas the B atoms should lie in the hollow sites [27]. As figure 6 (a) shows, there are two possible orientations that satisfy this but which are distinct due to the second layer of copper atoms: on the fcc hollow site there is no Cu atom in the second layer, whilst by contrast in the hcp site there is a Cu atom in the second layer immediately below the hollow site. The *h*-BN island on the left-hand side of figure 6(a) shows the N on the hcp site whilst the island on the right-hand side has N on the fcc site. DFT calculations indicate that the fcc site is preferable [27], although experimentally for *h*-BN Ni (111) it has been shown that the B atom can also stably sit on the hcp position [28]. The islands should have an edge parallel to the Cu $[\bar{1}10]$ direction as shown. The experimental results in figure 5 are thus consistent with this picture and show that both the fcc and hcp sites can be stable in this case. Note that as Auwärter *et al* explained for *h*-BN on Ni(111) [28], although the *h*-BN lattice has the same orientation in the fcc and hcp case the two islands cannot be seamlessly joined due to their different atomic registration and so linear

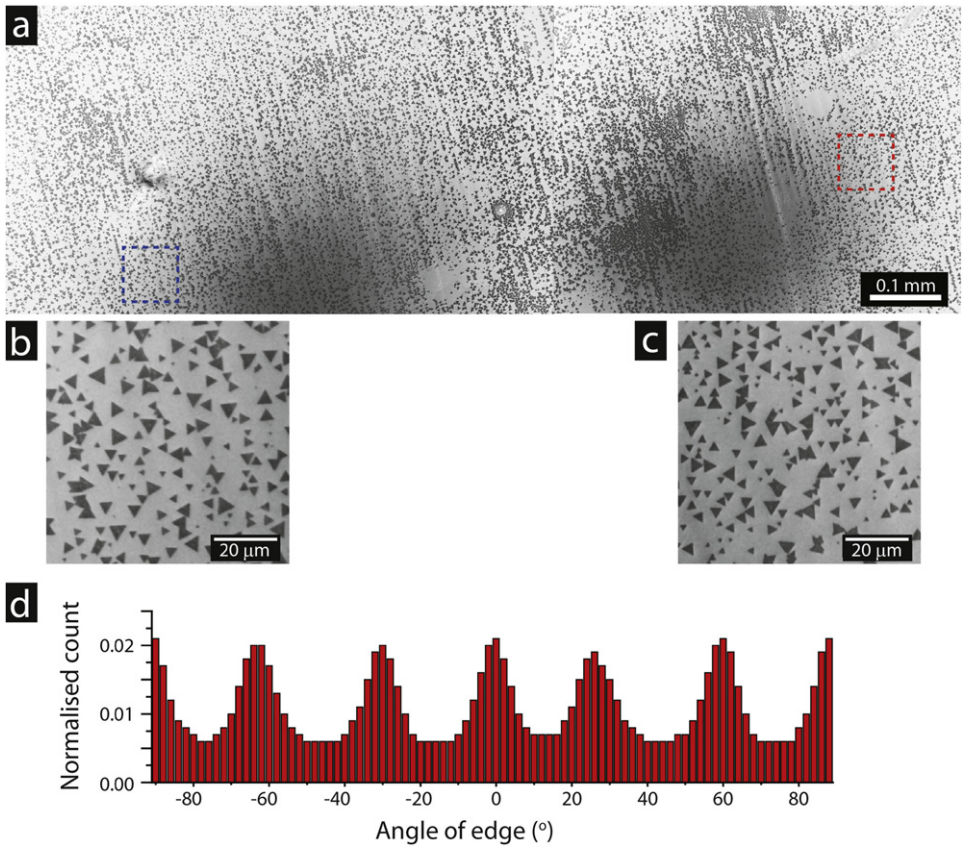

Figure 7. (a) Low magnification, high pixel density SEM image of *h*-BN islands on a single millimetre sized vicinal Cu(100) region of copper foil. Panels (b) and (c) show magnified sections of the image with clearly resolved triangular *h*-BN islands. The directionality histogram in (d) was obtained from the entire image and clearly shows peaks in edge orientation separated by 30°.

defects would be expected to mark the boundaries between two such domains. We note that in general comparison of the substrate surface lattice with the overlayer crystal structure is not the only factor that could define the orientation: for example, interactions between the edges of a growing island and the substrate surface could strongly influence the geometry, particular for the small island sizes where the orientation is first pinned.

On Cu(110), figure 6(b), the surface lattice is rectangular and so the match to the hexagonal *h*-BN is less clear. However, the rectangular Cu(110) surface has a periodicity of $a = a_{Cu}/\sqrt{2} = 0.255$ nm in one direction and hence can share a common periodicity with the *h*-BN. This would result in two (equivalent) favoured orientations of the *h*-BN islands aligned in the Cu $[\bar{1}00]$ / Cu [100] directions as shown.

The square lattice of the Cu(100) surface, with lattice parameter again $a = a_{Cu}/\sqrt{2} = 0.255$ nm, gives a lattice match in four different directions as shown in figure 6(c). This common periodicity could result in 4, equivalent, preferred orientations of the triangular *h*-BN islands with edges parallel to the Cu $[01\bar{1}]$ or Cu [011] direction as shown (i.e. rotated 90° relative to one another).

Figure 7 shows a large area of a substrate (more than 1 mm by around 0.5 mm) which EBSD showed to be a single copper grain with orientation vicinal Cu (100). The image was taken with a high pixel density and magnified views of the two areas highlighted by dashed squares are shown in figures 7(b) and (c). Visual inspection of these images suggests that four orientations are present. Directionality analysis of the entire SEM image in figure 7(a) is shown in figure 7(d) and clearly reveals a prevalence of edges separated by 30° from one another, consistent with the four island orientations rotated 90° from one another as shown in figure 6(c). Comparison with the EBSD data from the same area indicated that the island orientations were consistent with the expected copper crystallographic directions.

It is interesting to note that the epitaxial orientations determined here are different from those previously observed for LP-CVD of graphene on copper foil [15], where the graphene lattice was found to orient ±8° from the Cu[010] direction on Cu(100). The lattice parameter of graphene at room temperature is 0.246 nm, 3.6% less than a_{Cu} and 1.8% less than the *h*-BN lattice parameter. Accounting for thermal expansion, the lattice parameter of copper will be relatively larger at the growth temperature (as evidenced by the wrinkles in graphene and *h*-BN after growth). It appears that the difference in lattice parameter between graphene and *h*-BN is sufficient to result in

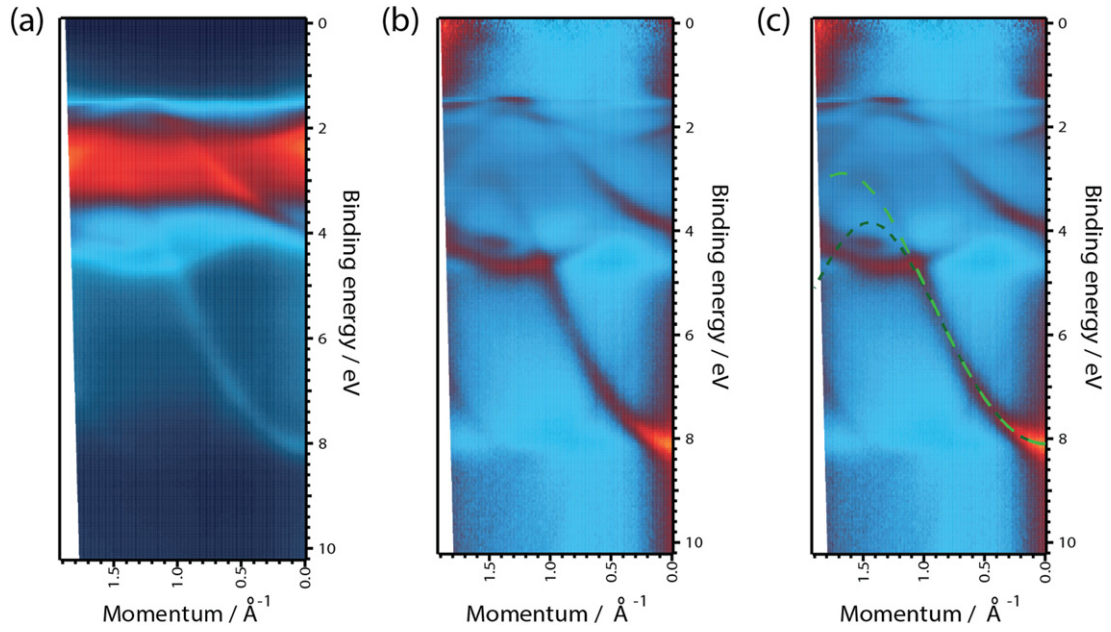

Figure 8. ARPES data from a full coverage *h*-BN sample. Left; raw image, centre; momentum distribution curve (MDC) normalized image, right; MDC normalized image with the dispersions of a tight-binding model for *h*-BN overlaid in green; the tight binding dispersion in the ΓM direction is the darker green line with shorter dashes, and in the ΓK direction is the lighter green line with longer dashes.

differences in their epitaxial alignment (i.e. misaligned from the high symmetry axis for graphene and aligned for *h*-BN), although the general phenomena of mismatch epitaxy and structural feedback/interfacial restructuring appear to be consistent for both graphene and *h*-BN on copper.

The clear epitaxial relation between *h*-BN and the copper surface indicates an interaction between the two. In order to gain insight into the strength of this interaction, and to determine the electronic quality of the *h*-BN, ARPES was used to measure the band-structure of the *h*-BN monolayer on copper foil. It should be noted that these measurements were taken after exposure to air, and hence some oxygen intercalation may have taken place [11]. The samples were annealed in UHV prior to measurement to return the samples to close to pristine condition, as measured by XPS. Figure 8 shows the dispersion of the *h*-BN bands measured on the copper foil. The orientation of the copper surface in this region is not known, but as the sample is predominantly vicinal Cu(100) we expect it to be Cu(100). The high intensity between 2 and 4 eV is due to the copper d states. In figure 8(b) the data has been modified by momentum distribution curve normalization (each line at constant energy is divided by the average of that line), making the *h*-BN π band dispersion more apparent. The *h*-BN valence band maximum is in the copper d states, but can be seen to be ~3 eV below the Fermi level consistent with a 6 eV band gap and similar to that found for *h*-BN on single crystal Cu(111) by Roth *et al* [19]. The dispersion can be approximately described by a nearest neighbour tight binding model, which is shown overlaid on the experimental data in figure 8(c). The tight binding model used is of the form

$$E\left(k_x, k_y\right) = \frac{\left(\varepsilon_B + \varepsilon_N\right)}{2} - \sqrt{\frac{\left(\varepsilon_B - \varepsilon_N\right)^2}{2} + 4t^2\left(\left(\cos\frac{k_y a}{2}\right)^2 + \cos\frac{\sqrt{3}k_x a}{2}\cos\frac{k_y a}{2} + \frac{1}{4}\right)}$$

with parameters: on site energies $\varepsilon_B = -\varepsilon_N$ =2.05 eV, hopping parameter t = 2.25 eV and lattice spacing a = 0.250 nm. The two dashed lines overlaid correspond to dispersion relations in the ΓM direction (darker green and shorter dashes) and the ΓK direction (lighter green and longer dashes). These represent the two limiting cases in the dispersion relation.

The dispersion of the *h*-BN is similar to that found by Roth *et al* on single crystal Cu(111), despite the different surface orientation of the copper here. The *h*-BN is electronically decoupled from the surface, maintaining its insulating character. This demonstrates that there is only a weak interaction between the copper surface and physisorbed *h*-BN monolayer.

4. Conclusions

As with graphene, the *h*-BN radically alters the surface topography and hence surface crystallography of the

copper, suggesting structural feedback between the overlayer and substrate. This occurs despite the interaction between the *h*-BN and copper being only weak, with ARPES showing that the *h*-BN is electronically decoupled from the copper surface, as expected in van der Waals epitaxy of a layered material such as *h*-BN. It is particularly surprising that this weak interaction is sufficient to induce epitaxial ordering, aligned to the high symmetry axes of the substrate, even when the symmetry of surface and overlayer are not matched. However, the degree of orientation is stronger on Cu(111), suggesting a stronger interaction when the symmetry is matched. The growth rate also appears to be faster on Cu(111) than Cu(100). For the cold-rolled copper foils studied here, which are predominantly Cu(100) after annealing, the four equivalent orientations of *h*-BN will lead to a prevalence of high angle (30°) grain boundaries. Controlling this epitaxy will enable the growth of high quality, large area, single crystal, monolayer *h*-BN films by low pressure CVD.

Acknowledgments

EPSRC is thanked for support through studentships to AJM and JJM and through grant number EP/K005200/1. We acknowledge support via the CALIPSO TransNational Access Program from the European Community's Seventh Framework Programme (FP7/2007-2013) under grant agreement number 312284.

References

[1] Yankowitz M, Xue J and LeRoy B J 2014 *J. Phys.: Condens. Matter* **26** 303201
[2] Nagashima A, Tejima N, Gamou Y, Kawai T and Oshima C 1995 *Phys. Rev.* B **51** 4606–13
[3] Li X *et al* 2009 *Science* **324** 1312–4
[4] Ismach A *et al* 2012 *ACS Nano* **6** 6378–85
[5] Gao Y, Ren W, Ma T, Liu Z, Zhang Y, Liu W B, Ma L P, Ma X and Cheng H M 2013 *ACS Nano* **7** 5199–206
[6] Tay R Y, Griep M H, Mallick G, Tsang S H, Singh R S, Tumlin T, Teo E H T and Karna S P 2014 *Nano Lett.* **14** 839–46
[7] Tay R Y, Wang X, Tsang S H, Loh G C, Singh R S, Li H, Mallick G and Tong Teo E H 2014 *J. Mater. Chem.* C **2** 1650
[8] Kim G, Jang A R, Jeong H Y, Lee Z, Kang D J and Shin H S 2013 *Nano Lett.* **13** 1834–9
[9] Han J, Lee J Y, Kwon H and Yeo J S 2014 *Nanotechnology* **25** 145604
[10] Gibb A L, Alem N, Chen J H, Erickson K J, Ciston J, Gautam A, Linck M and Zettl A 2013 *J. Am. Chem. Soc.* **135** 6758–61
[11] Kidambi P R, Blume R, Kling J, Wagner J B, Baehtz C, Weatherup R S, Schloegl R, Bayer B C and Hofmann S 2014 *Chem. Mater.* **26** 6380–92
[12] Huang P Y *et al* 2011 *Nature* **469** 389–92
[13] Liu Y, Zou X and Yakobson B I 2012 *ACS Nano* **6** 7053–8
[14] Koma A 1992 *Thin Solid Films* **216** 72–76
[15] Wilson N R *et al* 2013 *Nano Res.* **6** 99–112
[16] Murdock A T, Koos A, Britton T B, Houben L, Batten T, Zhang T, Wilkinson A J, Dunin-Borkowski R E, Lekka C E and Grobert N 2013 *ACS Nano* **7** 1351–9
[17] Brown L *et al* 2014 *Nano Lett.* **14** 5706–11
[18] Joshi S *et al* 2012 *Nano Lett.* **12** 5821–8
[19] Roth S, Matsui F, Greber T and Osterwalder J 2013 *Nano Lett.* **13** 2668–75
[20] Avila J, Razado-Colambo I, Lorcy S, Lagarde B, Giorgetta J L, Polack F and Asensio M C 2013 *J. Phys.: Conf. Ser.* **425** 192023
[21] Liu Y, Bhowmick S and Yakobson B I 2011 *Nano Lett.* **11** 3113–6
[22] Strudwick A J, Weber N E, Schwab M G, Kettner M, Weitz R T, Wünsch J R, Müllen K and Sachdev H 2015 *ACS Nano* **9** 31–42
[23] Sutter P and Sutter E 2014 *APL Mater.* **2** 092502
[24] Schneider C a, Rasband W S and Eliceiri K W 2012 *Nat. Methods* **9** 671–5
[25] Chen S, Cai W, Piner R D, Suk J W, Wu Y, Ren Y, Kang J and Ruoff R S 2011 *Nano Lett.* **11** 3519–25
[26] Wang Z J *et al* 2015 *ACS Nano* **9** 1506–19
[27] Laskowski R, Blaha P and Schwarz K 2008 *Phys. Rev.* B **78** 045409
[28] Auwärter W, Muntwiler M, Osterwalder J and Greber T 2003 *Surf. Sci.* **545** 735–40